as follows: VA units forming the PVA sequence, 92.0 mol %; 1,2-glycol linkages, 2.0 mol %; short branches, 0.4 mol %; CA units, 2.8 mol %; γ-lactone units, 1.4 mol %; VAc units, 1.4 mol%. Thus, the results from the 125.76-MHz ^{13}C NMR spectrum agreed with those from the 90-MHz ^{1}H NMR spectrum within experimental error.

Acknowledgment. We thank Dr. T. Moritani of Kuraray Co., Ltd., for preparing a number of PVA–CA copolymers. We are also grateful to Drs. E. Bartholdi and W. E. Hull of Bruker Spectrospin Co., Ltd., for measuring the 125.76-MHz ^{13}C NMR spectra. Special thanks are due to Professors Y. Fujiwara and J. W. Higgins of the University of Tsukuba for valuable comments.

References and Notes

(1) Hermann, W. O.; Haehnel, W. *Ber. Dtsch. Chem. Ges.* **1927**, *60*, 1658.
(2) Matsumoto, M. *Kobunshi Kagaku* **1950**, *7*, 142.
(3) Sakurada, I.; Kawashima, K. *Kobunshi Kagaku* **1951**, *8*, 142.
(4) Maruhashi, M.; Yamamoto, N.; Noro, K. The 24th Annual Meeting of Polymer Chemistry in Japan, Tokyo, 1972, Vol. 1A, p 7.
(5) (a) Johnson, R. N.; Loury, J. B.; Riggs, N. V. *Tetrahedron Lett.* **1967**, *50*, 5113. (b) Johnson, R. N.; Riggs, N. V. *Ibid.* **1967**, *50*, 5119.
(6) Kotani, M. "Daiyuuki-Kagaku"; Asakura: Tokyo, 1969.
(7) Ham, G. E. *J. Polym. Sci.* **1954**, *14*, 87.
(8) (a) Inoue, Y.; Chujo, R.; Nishioka, A.; Nozakura, S.; Iimuro, H. *Polym. J.* **1973**, *4*, 244. (b) Wu, T. K.; Sheer, M. L. *Macromolecules* **1977**, *10*, 529.
(9) Flory, P. J.; Leutner, F. S. *J. Polym. Sci.* **1948**, *3*, 880.
(10) Levy, G. C.; Nelson, G. L. "^{13}C Nuclear Magnetic Resonance for Organic Chemists"; Wiley-Interscience: New York, 1972.
(11) Roedel, M. T. *J. Am. Chem. Soc.* **1953**, *75*, 6110.
(12) Adelman, R. L.; Ferguson, R. C. *J. Polym. Sci., Polym. Chem. Ed.* **1975**, *13*, 891.
(13) (a) Morishima, Y.; Iimuro, H.; Nozakura, S. *J. Polym. Sci., Polym. Lett. Ed.* **1975**, *13*, 157. (b) Nozakura, S.; Morishima, Y.; Iimuro, H.; Irie, Y. *J. Polym. Sci., Polym. Chem. Ed.* **1976**, *14*, 759.

Structural Studies of Poly(ethylenimine). 2. Double-Stranded Helical Chains in the Anhydrate

Yozo Chatani,* Takushi Kobatake, and Hiroyuki Tadokoro

Department of Macromolecular Science, Faculty of Science, Osaka University, Toyonaka, Osaka 560, Japan

Ryuichi Tanaka

Graduate School of Engineering Science, Kyushu University, Hakozaki, Fukuoka 812, Japan. *Received July 10, 1981*

ABSTRACT: X-ray structural analysis of linear poly(ethylenimine) in the anhydrous state revealed that the polymer chains exist as double-stranded helices, distinct from the fully extended form in the sesquihydrate and the dihydrate. One molecular chain in the anhydrate takes practically a 5/1 helical form (five monomeric units per turn) with an identity period of 0.958 nm, and a pair of chains possessing the same helical sense forms a double strand with a relative rotation of 180° about the chain axis at the same level. The formation of the double-stranded helices in the anhydrate is ascribable to N–H···N hydrogen bonding between the two polymer chains in the double strand. The crystals of the anhydrate are orthorhombic, with cell dimensions a = 2.98 nm, b = 1.72 nm, and c (fiber axis) = 0.479 nm. The space group is D_{2h}^{24}-*Fddd*, and there are 40 monomeric units (8 strands) in the unit cell. The observed fiber period of 0.479 nm, which is half the length of the identity period of the 5/1 helix, is interpreted in terms of statistical dispositions of the strands; two diffuse layer lines interpreted by doubling the fiber period are well explained by this statistical structure. In more detail, the period estimated from the intervals of the diffuse layer lines is not exactly twice the fiber period; a 69/14 helical chain (4.93 monomeric units per turn) may be a better approximation, and probably the double strand has no periodicity. The large unit cell is interpreted in terms of hexagonal-like closest packing of the right-handed and left-handed strands. The X-ray diffraction study also revealed that a reversible transformation between the double-stranded helical chains and the extended chains on absorption of water vapor and dehydration is attained in the solid state, with retention of the orientation of the chain axis.

Linear poly(ethylenimine) (PEI) is remarkably hygroscopic; it exists as one of several hydrates or their mixture in air. In a previous paper,[1] we reported the crystal structures of two hydrates of PEI, viz., the sesquihydrate $(-CH_2CH_2NH-\cdot 1.5H_2O)_n$ and the dihydrate $(-CH_2CH_2NH-\cdot 2H_2O)_n$. The NH groups of PEI can behave as both proton donors and proton acceptors for hydrogen bonding, and, in fact, all of the NH groups in both hydrates participate in N–H···O and N···H–O hydrogen bonding with water, irrespective of the difference in their EI to water mole ratio. Therefore, the structure of the anhydrate and especially the behavior of the NH groups in the anhydrous state are of much interest. However, besides the hygroscopic feature, the low molecular weight PEI used in the previous study has made it difficult to prepare a uniaxially oriented specimen of the anhydrate, which is indispensable for the X-ray structure analysis. Recently, a high molecular weight PEI enabled us to prepare uniaxially oriented samples of the anhydrate by dehydration of uniaxially oriented samples of the hydrates, and X-ray structure analysis of the anhydrate revealed that the polymer chains exist as double-stranded helices.

Experimental Section

The sample used in this study was obtained from 2-phenyl-2-oxazoline, and the molecular weight was estimated to be about

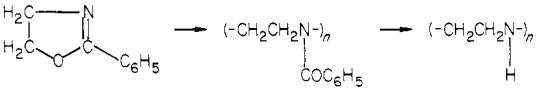

1×10^5. The details of the synthesis and polymer characterization will be reported elsewhere.[2] The original PEI sample was melted and dehydrated at about 100 °C in vacuo and was subjected to quenching in dry ice/methanol followed by stretching about five times. The sample thus obtained was highly oriented but tended

0024-9297/82/2215-0170$01.25/0

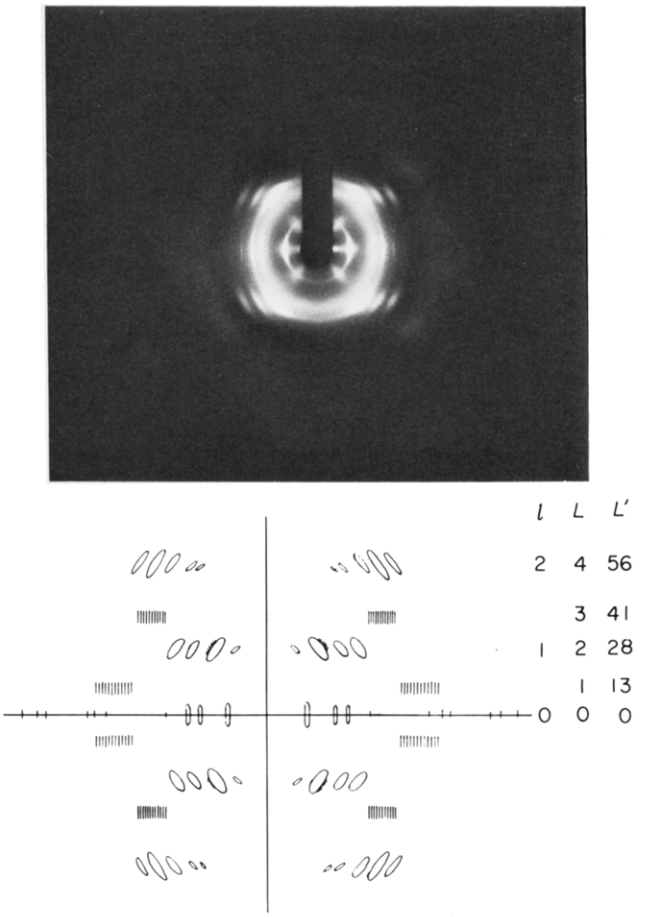

Figure 1. X-ray fiber diagram of the PEI anhydrate and its schematic representation.

to transform rapidly into the hydrates in air, even though the fresh specimen was the anhydrate. The oriented 0.3-mm-diameter specimen was then inserted into a thin-walled Lindemann glass capillary and was dehydrated by evacuation below the melting temperature of the anhydrate, 54 °C (in practice at 1.3×10^{-2} Pa at 30 °C for 2 days). After the dehydration, the capillary was sealed in vacuo. Figure 1 shows the X-ray fiber diagram of the anhydrate thus obtained together with a schematic representation; the diagram confirmed that the uniaxial orientation was retained as in the original hydrate, and the sample was free from any hydrates. The diffraction intensities were obtained with nickel-filtered copper Kα radiation by the multiple-film method and was estimated by visual comparison with a standard intensity scale. The reflection intensities for the powdery anhydrate sample were also measured with a diffractometer to estimate the intensity ratios among the layer lines because the reflections of layer lines are much broader than those of the equator. The density of the anhydrate was estimated by a flotation method in a 1,1,2,2-tetrachloroethane/cyclohexane mixture at 20 °C in such a way that the capillary containing the anhydrate specimen was broken in the mixture in order to prevent the sample from contacting with water vapor in atmospheric air. The density was observed to be 1.14×10^3 kg·m^{-3}.

Determination of Structure

The X-ray fiber diagram of the anhydrate is characterized by the following.

(1) The most intense reflection, with a long d spacing of 0.746 nm, which is the most obvious indication of the anhydrate, appears on the equator.

(2) Despite the sharp reflections on the equator, their intensities fade remarkably with increasing scattering angle. On the other hand, the reflections on layer lines are rather broad. Finally, only 22 reflections were observed in a long-exposure photograph.

(3) The fiber period, 0.479 nm, is quite different from that of 0.736 nm in both hydrates. However, as shown later, in a later stage of the analysis, two diffuse layer lines indicating twice the fiber period of 0.479 nm were detected in a long-exposure photograph.

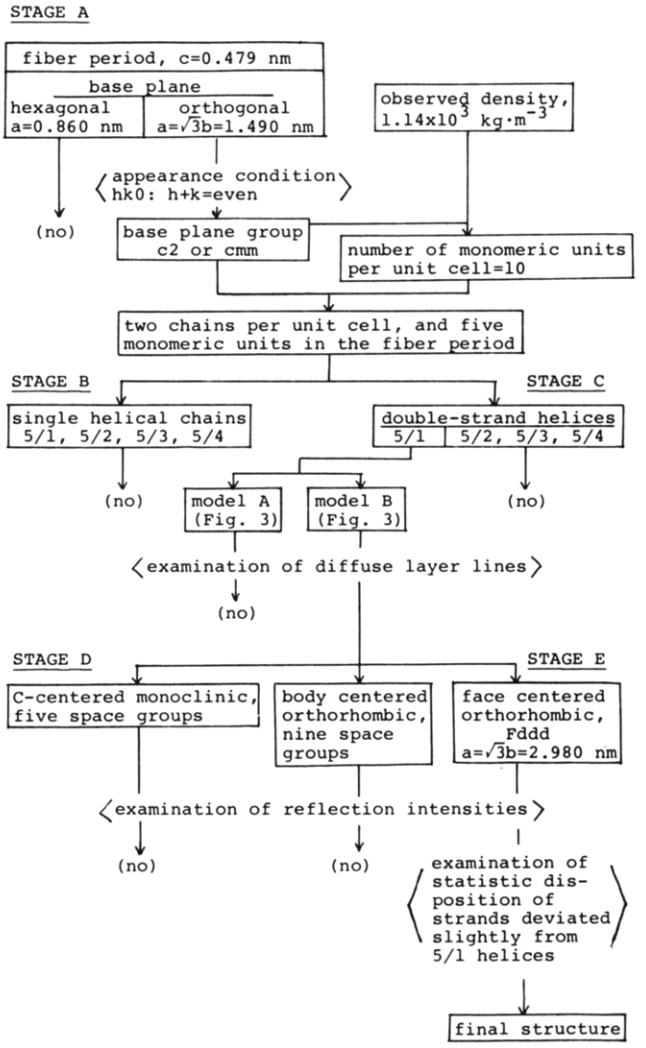

Figure 2. Flow chart of the structure analysis.

The process that led to the conclusion will be explained referring to the flow chart shown in Figure 2.

Stage A. The equatorial reflections are well indexed by a hexagonal cell with $a = 0.860$ nm or a base-centered orthogonal cell with $a = \sqrt{3}b = 1.490$ nm and $b = 0.860$ nm. However, the hexagonal cell and larger hexagonal cells are unable to account for the reflections on layer lines. The unit cell is then considered to be either orthorhombic or monoclinic with a base plane group of $c2$ or cmm. Next, referring to the observed density, the number of monomeric units per unit cell would be in the following range.

no. of monomeric units/unit cell	calcd density, kg·m^{-3}
8	0.93×10^3
9	1.05×10^3
10	1.16×10^3
11	1.28×10^3
12	1.40×10^3 [a]

[a] Cf. obsd 1.14×10^3 kg·m^{-3}.

The most reasonable value is 10; odd numbers 9 and 11 appear unreasonable because both plane groups $c2$ and cmm require an even number of monomeric units in the unit cell. The discrepancy between the observed and calculated densities is too large when the number is 8 or 12. Therefore, the only possible case would be that two polymer chains whose identity period consists of five monomeric units are located at the corner and the center of the unit cell.

Stage B. A geometrically permissible molecular model having 5/1 helical symmetry (five monomeric units per turn) with a fiber

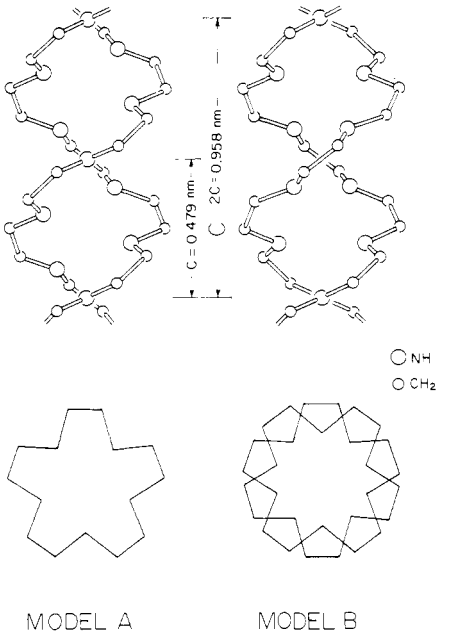

Figure 3. Two kinds of double-stranded helical chains of PEI. Model B was finally accepted.

period of 0.479 nm was analytically sought under the assumptions of a C–C bond length of 0.153 nm, a C–N bond length of 0.147 nm, all bond angles of 109.5°, and D_5 molecular symmetry; i.e., a twofold rotation axis perpendicular to the helical axis passes through each nitrogen atom and the middle point of each C–C bond, because the plane groups $c2$ and cmm require at least one mirror plane in the ab projection. The 5/1 helical model obtained consists of C–C bonds of nearly cis form and C–N bonds of nearly trans form, the radius of the helix of the carbon atoms being 0.33 nm. Two helical chains having such a large radius cannot be packed in the unit cell without too close $CH_2 \cdots CH_2$ contacts, and the strongest equatorial reflection cannot be explained at all by this structure. Other helices, 5/2, 5/3, and 5/4, are evidently excluded because too short atomic distances appear between adjacent turns of the helix.

Stage C. Then we had to consider double-stranded helices, in which one polymer chain is again a 5/1 helix but the identity period in this case is twice the observed fiber period. A double strand involving two chains having the same helical sense gives a fiber period of 0.479 nm as was observed when the two chains are equally separated along the chain axis (model A in Figure 3) (Appendix, eq 4). Other double strands composed of 5/2, 5/3, and 5/4 helices do not satisfy the observed fiber period and/or are infeasible from stereochemical aspects as stated for the single-chain models. This 5/1 helix has a small radius (about 0.27 nm for the carbon atoms), two double strands of model A can be packed well in the unit cell, and this structure can explain all of the equatorial $hk0$ reflection intensities except small discrepancies (Appendix, section b). However, at this stage we observed the diffuse layer lines interpreted by twice the fiber period as stated before. Model A cannot explain the long period. Another model, model B in Figure 3, was then considered. Model B again consists of 5/1 helices but in this case two chains are rotated by 180° about the chain axis at the same level, and hence the identity period of the double strand is 0.958 nm (Appendix, eq 6). Model B gives very good agreement between observed and calculated $hk0$ reflection intensities (Appendix, section b).

If model B was the case, a statistical structure should be taken into account in order to explain the fact that Bragg reflections appear only on the layer lines defined by the fiber period of 0.479 nm. Such a structure can be generated, most simply by locating strand B with equal probability at two heights separated by 0.479 nm, half of the identity period (Appendix, eq 10). This statistical structure would not disturb seriously the packing of the strands because of the similar structure at the two heights as can be understood from model B in Figure 3, and this statistical disposition can be achieved in practice not by a shift of 0.479 nm but by a screw displacement of the double strand with a rotation of $2\pi/10$ and a shift of 0.958/10 nm along the chain axis.

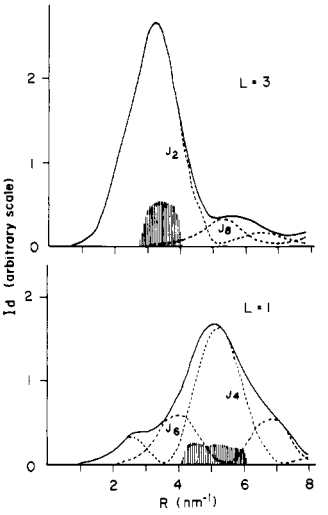

Figure 4. Observed (hatched area) and calculated (solid curves) diffuse scattering intensities for $L = 1$ and 3. As for broken curves, see Appendix, section d.

This statistical structure can explain the experimental fact that Bragg reflections appear only on the layer lines of 0.479-nm period. In addition, the intensities of the diffuse layer lines for this structure were calculated (Appendix, eq 16). The result is compared with the observed data in Figure 4. The position of intensity maxima and the relative intensities of the two layer lines are explained, qualitatively but well, by this structure.

Stage D. Since the observed Bragg reflections are few, the crystal symmetry could not be decided uniquely from systematic absences of the reflections. However, the unit cell appears to be a body-centered orthorhombic cell, with $a = 1.490$ nm, $b = 0.860$ nm, and $c = 0.479$ nm, or a C-centered monoclinic cell, with either $a = 1.565$ nm, $b = 0.860$ nm, $c = 0.479$ nm, and $\beta = 107.8°$ or $a = 0.984$ nm, $b = 1.490$ nm, $c = 0.479$ nm, and $\beta = 119.1°$. Nine space groups of the body-centered orthorhombic cell are $I222$, $I2_12_12_1$, $Imma$, $Iba2$, $Ima2$, $Immm$, $Ibam$, $Ibca$, and $Imma$, while five space groups for the monoclinic cells are $C2$, Cm, Cc, $C2/m$, and $C2/c$. The crystal structure of the anhydrate was examined for all of these space groups. Several space groups, $C2/c$, $Immm$, and $Imma$, explained roughly the observed reflection intensities of layer lines but left discrepancies, especially for a few nonobserved reflections. These examinations, however, gave us information that better agreement is obtained when the unit cell is composed of right-handed and left-handed strands disposed in a statistical way not conforming to the symmetry of the space groups. This fact induced us to reexamine the space group of this crystal.

Stage E. Finally we had to consider the larger unit cell of the space group $Fddd$, which has twice the a and b dimensions of the body-centered orthorhombic cell. The finally accepted crystal data are as follows: crystal system, orthorhombic; space group, D_{2h}^{24}-$Fddd$; cell constants, $a = 2.98$ nm, $b = 1.72$ nm, $c = 0.479$ nm; number of monomeric units per unit cell, 40 (8 strands). Although the new unit cell gives Miller indices different from those of the body-centered cell, the positions of the observed reflections are essentially the same for both cells. The $Fddd$ crystal lattice explained the relative intensities on each layer line very well; the discrepancies that we met in the cases of the body-centered cell and the C-centered cells were entirely removed. The calculated structure factors of the first ($l = 1$) and second ($l = 2$) layer lines are, however, considerably larger than those of the equator as shown in Figure 5a (the R factor, $\sum|I_o^{1/2} - I_c^{1/2}|/\sum I_o^{1/2}$, where $I = \sum mF^2$, for the raw data shown in Figure 5a was 0.15, where an isotropic thermal parameter, B, of 0.1 nm^2 was assumed, and after fitting the scale for all the layer lines, the R factor was 0.14). Motional or dispositional disorders characteristic of helical polymers might be invoked with rotation about the helix axis and screw displacement along the helical chain, and these disorders will be capable of reducing the intensities of nonequatorial reflections. As one of the extreme cases, the helical chain exhibiting a large degree of disorder with respect to screw displacement can

Table I
Fractional and Cylindrical Atomic Coordinates of the PEI Anhydrate [a]

atom	x	y	z	r, nm	ϕ, deg	z, nm
N	0.0000	0.0901	0.0000	0.155	0.0	0.0000
C	0.0352	0.1436	0.0983	0.267	23.2	0.0471
H of NH	0.011	0.058	−0.155	0.105	18.4	−0.074
H of CH_2	0.020	0.192	0.205	0.335	10.0	0.098
H of CH_2	0.054	0.162	−0.081	0.322	30.0	−0.039

[a] Equivalent atoms in the monomeric unit are located at $(-x, y, -z)$. Coordinates of other monomeric units are defined by 5/1 helical symmetry. As for the NH hydrogen atom, see the discussion section.

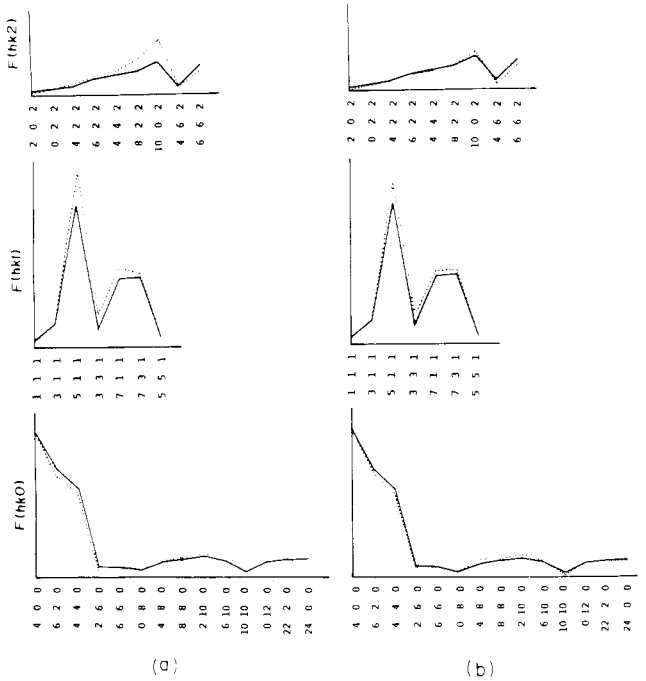

Figure 5. Observed (solid lines) and calculated (dotted lines) structure factors: (a) double strand of 5/1 helices; (b) double-stranded wire model. For simplicity, only one set of Miller indices is given for each reflection.

be replaced by a continuous wire model. The structure factor of the wire model instead of the 5/1 helix in the *Fddd* lattice was calculated (Appendix, section e), in which a correction for the thermal motion of the form $\exp[-B_r(R/2)^2 - n^2\Delta\phi^2/2]$[4,5] was applied, where the first and second terms are for displacement along the radial direction and rotational displacement about the helix axis, respectively. Figure 5b shows the observed and calculated structure factors for the wire model, where $B_r = 0.07$ nm^2 and $\Delta\phi = 12°$ were assumed. The continuous wire model reduced the R factor to 0.12.

However, such a large thermal motion is probably apparent because the two diffuse layer lines are not exactly interpreted by twice the fiber period of 0.479 nm. The ζ values for the diffuse layer lines of $L = 1$ and 3 are smaller than 0.161 and 0.483, respectively, expected for the 5/1 helix as shown below.

l	L	ζ_{obsd}	
	1	0.148	diffuse
1	2	0.321	Bragg reflections
	3	0.469	diffuse
2	4	0.641	Bragg reflections

This implies that the polymer chains slightly deviate from the 5/1 helix, and such a structure has been found for many helical polymers.[6-9] From these ζ values, a 69/14 (4.93 monomeric units per turn) helix seems a better approximation, and probably the strand has no periodicity (Appendix, section f). Accordingly, it is conceivable that the characteristic features, i.e., the fiber period of the half-identity period, the appearance of diffuse layer lines, and the large thermal parameters, are caused by disorder with respect to the packing of the strands of the helices deviating from the 5/1 helix. That is, if nitrogen atoms can be disposed, with

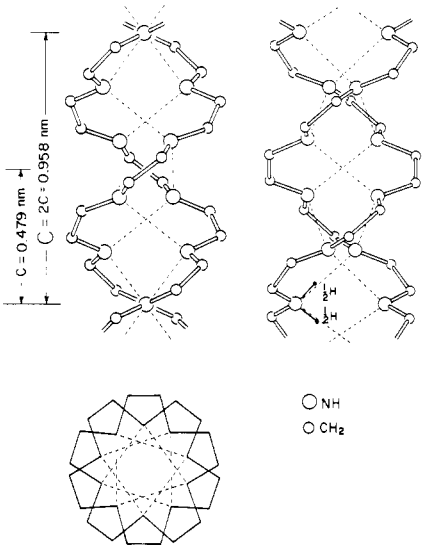

Figure 6. Double-stranded helical chains of PEI viewed along three perpendicular directions. Broken lines indicate N-H···N hydrogen bonds.

equal probability, at $y = 0$ at each lattice point separated by $c = 0.479$ nm along the chain axis, the strands of the helices slightly deviating from the 5/1 helix exhibit a disorder with respect to the orientation about the chain axis, and this effect on the X-ray diffraction might be similar to the large thermal motion mentioned above; no abnormality was found in DSC thermogram of the anhydrate from the melting temperature to ~175 °C. Such a slight deviation of the helical conformation, of course, does not affect seriously the result of the analysis for the 5/1 helix (Appendix, sections d and f). The atomic coordinates for the 5/1 helix are listed in Table I. Observed and calculated structure factors are listed in Table II. In the calculation of structure factors, the hydrogen atoms are included assuming C-H and N-H bond lengths of 0.109 and 0.098 nm, respectively.

Results and Discussion

Molecular Conformation. The most impressive feature of the structure of the PEI anhydrate is that the polymer chains exist as double-stranded helices (Figure 6). Each polymer chain is practically a 5/1 helix, the identity period of which is 0.958 nm. Two chains having the same helical sense form a double strand with a relative rotation of 180° about the helix axis at the same level (corresponds to model B in Figure 3). The chain conformation in the anhydrate is therefore quite different from the fully extended zigzag form in both hydrates.[1] The contraction of the helical chain from the extended form is ascribable to the near-cis conformation about the C–C bonds. The molecular dimensions derived from the atomic coordinates in Table II are as follows: bond lengths, C–C = 0.153 nm, C–N = 0.146 nm; bond angles, C–C–N = 112°, C–N–C = 104°; internal rotation angles, C–C = 13°, C–N = 160°.

The closest interchain atomic distances in the double strand, 0.396 and 0.417 nm for C···C pairs and 0.310 and 0.316 nm for N···N pairs, are comparable to twice the van

Table II
Observed and Calculated Structure Factors of the PEI Anhydrate

hkl	F_o	$F_{c,a}$[a]	$F_{c,b}$[a]
400, 220	690	684	718
620, 040	509	471	479
440, 800	416	392	378
260, 840, 10,2,0	50	29	38
660, 12,0,0	47	34	37
080, 12,4,0	25	28	29
480, 10,6,0, 14,2,0	63	70	88
880, 16,0,0	80	86	86
2,10,0, 14,6,0, 16,2,0	92	109	106
6,10,0, 12,8,0, 18,2,0	72	89	71
10,10,0, 20,0,0		51	13
0,12,0, 18,6,0, 20,4,0, 16,8,0, 4,12,0	70	97	71
22,2,0, 14,10,0, 8,12,0	82	81	83
24,0,0, 12,12,0, 20,8,0, 22,6,0	89	51	71
111		40	43
311	118	110	104
511, 131	665	812	777
331	w	150	142
711, 531	317	369	352
731, 151, 351, 911	325	338	361
551		54	23
202		3	0
022, 222		17	13
422, 602		54	50
622, 242	78	88	73
442	95	106	82
822, 642	110	167	104
10,0,2, 10,2,2, 842, 062, 262	160	256	183
462		34	10
662, 10,4,2, 12,2,2	138	102	104

[a] $F_{c,a}$ is the calculated structure factor for the double strand of 5/1 helices, and $F_{c,b}$ is for the double-stranded wire model, where F means $(\Sigma mF^2)^{1/2}$.

der Waals radius (0.155 nm for the N atom and 0.2 nm for the CH_2 group). From this point of view, the double strand is very tight. On the other hand, published data for N–H···N hydrogen bond distances scatter between 0.29 and 0.34 nm;[4] this implies that the N–H direction should be examined when the N···N distance is longer than twice the van der Waals radius of the N atom, 0.31 nm. Therefore, we shall examine whether N–H···N hydrogen bonds are attainable or not in the double strand.

Hydrogen Bonding. Considerable information on three crystalline forms of PEI, i.e., the anhydrate, the sesquihydrate, and the dihydrate, has now become available. As previously mentioned,[1,3] the nitrogen atoms assume a pyramidal structure like ammonia, and indeed the NH hydrogen atoms in the hydrates are located in this way. In both hydrates, every NH group participates in N–H···O and N···H–O hydrogen bonding, the mean hydrogen bond distance being 0.295 nm in the sesquihydrate and 0.293 nm in the dihydrate. For the double-stranded helices in the anhydrate, the shortest N···N distance, 0.310 nm, is found between two interchain nitrogen atoms lined up on the diameter of the strand. However, from the consideration of the N–H direction, this contact is not due to the N–H···N hydrogen bond but the closest van der Waals contact of the nitrogen atoms. The N–H direction is almost parallel to the second nearest N···N vector, 0.316 nm, as shown in Figure 6. The angle between the N–H bond and the N···N vector is less than 5° when the nitrogen bond angles are tetrahedral, and this nonlinearity of the N–H···N hydrogen bond would be in a fully acceptable range. Besides the X-ray evidence, from this viewpoint model A seems inadequate because there are no N–H vectors indicating the possibility of N–H···N hydrogen bonding.

The NH hydrogen atom would be located at two equivalent sites by nitrogen inversion;[1,3] there seems to be no evidence that the NH hydrogen atoms are located regularly in an isotactic or syndiotactic disposition in one polymer chain in solutions or the melt. In the course of formation of the double strand, however, the NH hydrogen atoms would be cooperatively disposed in a regular fashion so as to create as many N–H···N hydrogen bonds as possible except a few defects generated by thermal agitation. This situation may be similar to the behavior of H_2O hydrogen atoms in ice.

The network of N–H···N hydrogen bonds in the double strand is shown in Figure 6; all of the NH hydrogen atoms are thus able to participate in hydrogen bonding. We can therefore attribute the formation of the double strand to N–H···N hydrogen bonds. The high torsional energy due to the nearly cis form of the C–C bonds may be compensated by the formation of hydrogen bonds. In an α helix,[5] adjacent turns of the helix are held together by N–H···O hydrogen bonds, but they are intrachain ones. Different from the α helix, the N–H···N hydrogen bonds in the PEI anhydrate are interchain ones. In isotactic poly(methyl methacrylate),[6] the formation of a double strand (each polymer chain is a 10/1 helix) is attributable to the spatial fitting of two chains through the van der Waals interactions. The structure we propose for PEI is, therefore, the first known example among synthetic polymers of double-stranded helices stabilized by interchain hydrogen bonds.

Packing of Strands. The small number of observable reflections hindered a detailed structural analysis. This feature might be, conversely, an indication of the irregularity in packing of the strands to some extent and can be interpreted, as stated in the analytical section, by the

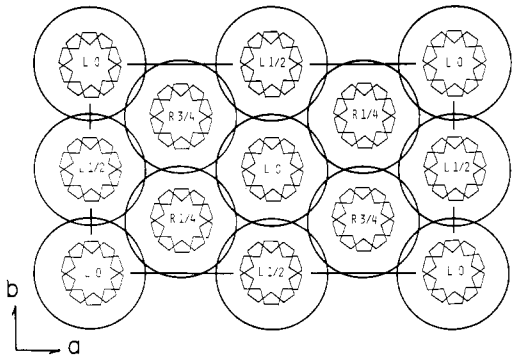

Figure 7. Packing of the double strands in the PEI anhydrate viewed along the chain axis. R and L indicate right-handed and left-handed strands, respectively. Numbers indicate the fractional heights of strands.

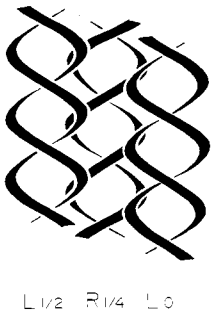

Figure 8. Schematic side view of the packing of double strands in the PEI anhydrate. Letters and numbers have the same meaning as in Figure 7.

statistical disposition of the strands of the helices slightly deviating from the 5/1 helix. The space group of the PEI anhydrate is *Fddd*, and probably this is the first case in which a polymer takes this space group. It will be understood, however, why the PEI anhydrate does take the large unit cell of *Fddd*. When $a = \sqrt{3}b$, this space group will enable the rod-shaped strands to pack in a hexagonal closest packing. Of course, optically active polymers, including native polymers, do not take this space group, since the *Fddd* lattice is achiral. In the PEI anhydrate, one right-handed strand is surrounded by two right-handed strands and four left-handed strands, and vice versa as shown in Figure 7. However, if the nearest-neighboring strands are located at the same height, the CH_2 groups come into too close contacts, and this situation may be seen in Figure 7 by the overlapping of the CH_2 van der Waals shells by about 0.07 nm. The nearest-neighboring strands along the *b* axis, which take the same helical sense, shift by $c/2$ (0.24 nm), while the nearest neighbors along the *ab* diagonal, possessing the opposite sense, shift by $c/4$ (0.12 nm) in the *Fddd* lattice. Figure 8 illustrates that these shifts bring about the most appropriate spatial fitting of right-handed and left-handed strands; the interstrand atomic distances are thus in an acceptable range, even if the orientation of chains about the helix axis distributes to some extent due to the deviation of the chain conformation from the 5/1 helix.

Transition between the Double-Strand Form and the Extended Form. As shown in Figure 6, NH groups make up the core of the double strand, whereas the strand is entirely covered with hydrophobic CH_2 van der Waals shells. Nevertheless, PEI exhibits a remarkable hygroscopic feature: the polymer chains readily undergo a transformation from the double-strand form to the fully extended form by absorption of water vapor in the solid state. If we employ a molecular model or threads, the dissociation of the double strand itself seems to be not so difficult, providing there are some functions which act to break the N–H···N hydrogen bonds. These functions are considered as follows. Free NH groups, which are thought to exist at the ends of strand, or local defects would be easily attacked by water, and the dissociation of the strand propagates as a "zipper effect". Besides such a effect, a long-range dipole interaction between water and the NH group might act over the CH_2 van der Waals shells and break the N–H···N hydrogen bonds. The morphological change in passing through the transition will be therefore of much interest.

Conclusion

This series of studies on PEI has revealed that the polymer chains transform between double-stranded helices and the fully extended form by dehydration and absorption of water, and especially the behavior of the NH groups in the anhydrate and the hydrates is revealed to some extent. In the course of this study, we found another hydrate besides the sesquihydrate and dihydrate, and the structure is now under study.

The conventional PEI prepared from ethylenimine has many types of branches and hence is an amorphous or sticky fluid, but the structures of the hydrates and anhydrate may be adoptable as the models for the local structures in the noncrystalline PEI. Finally, structural information on the polymorph of PEI will be basically available to elucidate the interesting functions of PEI on many industrial, agricultural, and medical purposes.[13]

Acknowledgment. We express our sincere thanks to Dr. Y. Morishima of Osaka University for his kind discussion.

Appendix

(a) The notations in the physical space and reciprocal space expressed in terms of the fiber period of 0.479 nm and the identity period of the 5/1 helix, i.e., twice the fiber period, will be discriminated by small letters c and l/c and capital letters C and L/C, respectively. Cylindrical coordinates in the physical space and reciprocal space are therefore expressed by (r,ϕ,z) and $(R,\psi,l/c)$ or $(R,\psi,L/C)$, respectively.

The Fourier transform of model A in Figure 3, F_A, is expressed in terms of the Fourier transform of the 5/1 helix, F_m, as

$$F_A(R,\psi,L/C) = F_m[1 + \exp(i\pi L)] \quad (1)$$

According to Cochran, Crick, and Vand[14]

$$F_m = \sum_n \sum_j f_j J_n(2\pi R r_j) \exp\{i[n(\pi/2 - \phi_j + \psi) + 2\pi L z_j/C]\} \quad (2)$$

$$L = n + 5m \qquad (m\text{: integers}) \quad (3)$$

where f is the atomic scattering factor and J_n is a Bessel function of the nth order. Equation 3 is the constrained condition for the orders (n) of the Bessel functions which should be taken into account in eq 2. From eq 1

$$F_A = 2F_m \quad \text{when } L \text{ is even}$$
$$F_A = 0 \quad \text{when } L \text{ is odd} \quad (4)$$

Namely, the fiber period is reduced to $C/2 = c$. On the other hand, for model B in Figure 3

$$F_B = F_m[1 + \exp(in\pi)] \quad (5)$$

F_B is not zero for all L layer lines, but from eq 5, Bessel functions of odd orders should be eliminated in the calculation of F_m in eq 6.

$$F_B = 2F_m \quad (6)$$

(b) On the equatorial reflections for model A (e.g., $\phi_N = 0$)

$$F_A(R,\psi,0) = A + iB$$

$$A = 2f_N J_0(2\pi R r_N) + 4f_C J_0(2\pi R r_C) - 4f_N J_{10}(2\pi R r_N) \cos 10\psi - 8f_C J_{10}(2\pi R r_C) \cos 10\psi \cos 10\phi_C$$

$$B = 4f_N J_5(2\pi R r_N) \cos 5\psi + 8f_C J_5(2\pi R r_C) \cos 5\psi \cos 5\phi_C \quad (7)$$

As for model B, since the term B in eq 7 should be eliminated from eq 5,

$$F_B(R,\psi,0) = A \quad (8)$$

The contribution of the term B in eq 7 increases the calculated intensities for very weak reflections. From this point of view, model B is preferable.

(c) For the statistical structure in which the double strand of model B is disposed at $z = 0$ and $C/2 = c$ with equal probability

$$\langle F_B \rangle = \tfrac{1}{2} F_B[1 + \exp(i\pi L)] \quad (9)$$

Therefore

$$\langle F_B \rangle = F_B \quad \text{when } L \text{ is even}$$
$$\langle F_B \rangle = 0 \quad \text{when } L \text{ is odd} \quad (10)$$

This implies that such a statistical structure gives Bragg reflections only on layer lines expressed in terms of the fiber period of c, 0.479 nm. In this case again, Bessel functions of even orders should be considered in the calculation of F_B.

(d) The diffuse scattering intensity, I_d, is expressed as

$$I_d = \langle F^2 \rangle - \langle F \rangle^2 \quad (11)$$

For the layer lines $L = 1$ and 3, $\langle F \rangle = 0$ from eq 10. Therefore

$$I_d = \langle F^2 \rangle \quad (12)$$

where Bessel functions of even orders should be taken into account for model B, i.e., for $L = 1$, J_4 and J_6, while for $L = 3$, J_2 and J_8 were included. To a good approximation, the diffuse scattering intensities on the fiber diagram are expressed in terms of the squares of the Fourier transform of the double strand of model B averaged on ψ.

$$I_d = \langle F_B^2 \rangle_\psi = \int_0^{2\pi} \sum_j \sum_{j'} \sum_n \sum_{n'} f_j f_{j'} J_n(2\pi R r_j) J_{n'}(2\pi R r_{j'}) \times \exp\{i[(n - n')\psi + (n'\phi_{j'} - n\phi_j) + (n - n')\pi/2 + 2\pi L(z_j - z_{j'})/C]\}\, d\psi \quad (13)$$

Since

$$\int_0^{2\pi} \exp[i(n - n')\psi]\, d\psi = 0 \quad \text{when } n \neq n' \quad (14)$$

eq 13 becomes

$$I_d = \sum_j \sum_n f_j^2 J_n^2(2\pi R r_j) + 2 \sum_{j \neq j'} \sum_n f_j f_{j'} J_n(2\pi R r_j) J_n(2\pi R r_{j'}) \times \cos[n(\phi_{j'} - \phi_j) + 2\pi L(z_j - z_{j'})/C] \quad (15)$$

Since n is even for model B, eq 15 becomes

$$I_d = \sum_n \left(\sum_j f_j J_n(2\pi R r_j) \cos[-n\phi_j + 2\pi L z_j/C]\right)^2 \quad (16)$$

This implies that the contribution of Bessel functions of different orders are incoherent. The calculated intensities for $L = 1$ and 3 are shown in Figure 4 by solid curves, and broken curves in the figure indicate each component in eq 16 with respect to the order of the Bessel function.

(e) The Fourier transform of a continuous wire was given by Cochran et al.[14] Only one Bessel function, whose order is the same as the order of a layer line, L, contributes in this case. Accordingly, the structure factor of the double-stranded wire model for the *Fddd* lattice is given as follows.

For $l = L = 0$

$$F(hk0) = 40 \sum_j f_j J_0(2\pi R r_j) \quad (17)$$

For $l = 1$ ($L = 2$)

$$F(hk1) = A + iB \quad (18)$$

$$A = \pm B = -20 \sum_j f_j J_2(2\pi R r_j) \cos(4\pi z/C) \times \{\cos[2(\psi - \pi/2)] \pm \sin[2(\psi - \pi/2)]\} \quad (19)$$

where the plus and minus signs are for $h + k + l = 4n + 1$ and $4n + 3$, respectively.

For $l = 2$ ($L = 4$)

$$F(hk2) = 40 \sum_j f_j J_4(2\pi R r_j) \cos(8\pi z/C) \cos[4(\psi - \pi/2)] \quad \text{for } h + k + l = 4n \quad (20)$$

$$F(hk2) = 40i \sum_j f_j J_4(2\pi R r_j) \cos(8\pi z/C) \sin[4(\psi - \pi/2)] \quad \text{for } h + k + l = 4n + 2 \quad (21)$$

where z means the height of a wire at $\phi = 0$ ($x = 0$) (for the wire of nitrogen, $z = 0$) and the summation in eq 17–21 is made for all the atoms in the monomeric unit.

(f) The deviation of the conformation from the 5/1 helix to the 69/14 helix brings about splitting of the layer lines. According to the constrained condition in the helical equation for the two kinds of helices, $L = n + 5m$ and $L' = 14n' + 69m'$, the diffuse layer lines noticed, $L = 1$ and 3 for the 5/1 helix should be split for the 69/14 helix as shown below.

order of Bessel function, $n = n'$	layer line for 5/1 helix		layer line for 69/14 helix	
	L	ζ_{calcd}	L'	ζ_{calcd}
4	1	0.161	13	0.149
6	1	0.161	15	0.172
2	3	0.483	41	0.470
8	3	0.483	43	0.493

Since the intensities of diffuse layer lines $L = 1$ and 3 of the 5/1 helix are mainly attributed to Bessel functions of $n = 4$ and 2, respectively, as shown in Figure 4 (broken lines), the diffuse layer lines for the 69/14 helix are shifted to smaller ζ values as observed experimentally.

References and Notes

(1) Chatani, Y.; Tadokoro, H.; Saegusa, T.; Ikeda, H. *Macromolecules* **1981**, *14*, 315.
(2) Tanaka, R., to be published.
(3) Chatani, Y. Abstracts of U.S.–Japan Polymer Symposium, Palm Springs, 1980. *Contemp. Top. Polym. Sci.*, in press.
(4) Clark, E. S.; Muus, L. T. *Z. Kristallogr.* **1962**, *117*, 108.
(5) Takahashi, Y.; Tadokoro, H. *J. Polym. Sci., Polym. Phys. Ed.* **1979**, *17*, 123.
(6) Franklin, R. E.; Klug, A. *Acta Crystallogr.* **1955**, *8*, 777.
(7) Brown, L.; Trotter, L. F. *Trans. Faraday Soc.* **1956**, *52*, 537.
(8) Chatani, Y. *J. Polym. Sci.* **1960**, *47*, 491.
(9) Carazzolo, G. A. *J. Polym. Sci., Part A* **1963**, *1*, 1573.
(10) Nyburg, S. C. "X-Ray Analysis of Organic Structures"; Academic Press: New York, 1961; p 306.
(11) Pauling, L.; Corey, R. B.; Branson, H. R. *Proc. Natl. Acad. Sci. U.S.A.* **1951**, *37*, 205.
(12) Kusanagi, H.; Tadokoro, H.; Chatani, Y. *Macromolecules* **1976**, *9*, 531.
(13) Ham, G. H. *Encyl. Polym. Sci. Technol.* **1976**, *Suppl. 1*, 25.
(14) Cochran, W.; Crick, F. H. C.; Vand, V. *Acta Crystallogr.* **1952**, *5*, 581.